The Journal of Experimental Biology 210, 1912-1924
Published by The Company of Biologists 2007
doi:10.1242/jeb.002063

Low speed maneuvering flight of the rose-breasted cockatoo (*Eolophus roseicapillus*). II. Inertial and aerodynamic reorientation

T. L. Hedrick[1,*], J. R. Usherwood[2] and A. A. Biewener[3]

[1]*Department of Biology, CB 3280 Coker Hall, University of North Carolina, Chapel Hill, NC 27599-3280, USA,*
[2]*Structure and Motion Laboratory, The Royal Veterinary College, North Mymms, Herts, AL9 7TA, UK and*
[3]*Concord Field Station, MCZ, Harvard University, Old Causeway Road, Bedford, MA 01730, USA*

*Author for correspondence (e-mail: thedrick@bio.unc.edu)

Accepted 6 March 2007

Summary

The reconfigurable, flapping wings of birds allow for both inertial and aerodynamic modes of reorientation. We found evidence that both these modes play important roles in the low speed turning flight of the rose-breasted cockatoo *Eolophus roseicapillus*. Using three-dimensional kinematics recorded from six cockatoos making a 90° turn in a flight corridor, we developed predictions of inertial and aerodynamic reorientation from estimates of wing moments of inertia and flapping arcs, and a blade-element aerodynamic model. The blade-element model successfully predicted weight support (predicted was 88±17% of observed, *N*=6) and centripetal force (predicted was 79±29% of observed, *N*=6) for the maneuvering cockatoos and provided a reasonable estimate of mechanical power. The estimated torque from the model was a significant predictor of roll acceleration (r^2=0.55, *P*<0.00001), but greatly overestimated roll magnitude when applied with no roll damping. Non-dimensional roll damping coefficients of approximately –1.5, 2–6 times greater than those typical of airplane flight dynamics (approximately –0.45), were required to bring our estimates of reorientation due to aerodynamic torque back into conjunction with the measured changes in orientation. Our estimates of inertial reorientation were statistically significant predictors of the measured reorientation within wingbeats (r^2 from 0.2 to 0.37, *P*<0.0005). Components of both our inertial reorientation and aerodynamic torque estimates correlated, significantly, with asymmetries in the activation profile of four flight muscles: the pectoralis, supracoracoideus, biceps brachii and extensor metacarpi radialis (r^2 from 0.27 to 0.45, *P*<0.005). Thus, avian flight maneuvers rely on production of asymmetries throughout the flight apparatus rather than in a specific set of control or turning muscles.

Key words: avian, maneuvering, biomechanics, flight, dynamics, *Eolophus roseicapillus*.

Introduction

Birds and other flapping fliers have long been noted for their agility in flight, especially in comparison with fixed wing aircraft. While much of the difference in apparent maneuverability is no doubt a product of the lower wing loading and therefore greater ‘intrinsic’ maneuverability of biological fliers (Warrick et al., 1998), some may be due to means of reorientation available to flapping fliers but not to fixed wing aircraft. Changes in roll orientation and the resulting redirection of net aerodynamic force form the basis for changes in flight path or direction in many flying animals, including pigeons (Warrick and Dial, 1998), cockatoos (Hedrick and Biewener, 2007b), bats (Aldridge, 1987), houseflies (Wagner, 1986) and fruit flies (Fry et al., 2003), as well as fixed wing aircraft. Therefore, mechanisms for changing roll orientation may strongly influence maneuvering performance. In addition to changes in orientation due to external forces such as aerodynamic torques acting on the wings, flapping fliers may also reorient *via* inertia, much as a cat does when dropped from a height (e.g. Frohlich, 1980). In flapping flight, right–left asymmetry in the arcs swept by the two wings leads to instantaneous changes in body orientation. When the moments of inertia of the wings and body do not vary through the stroke cycle, these inertial reorientations lead to no net change over the course of a complete wingbeat cycle. However, in vertebrate fliers with jointed wings capable of changes in moment of inertia about each axis throughout the stroke, net inertial reorientations may also occur and contribute to maneuvering performance.

Here, we use a blade-element aerodynamic model of force production to estimate the aerodynamic torques and resulting changes in orientation generated by turning cockatoos *Eolophus roseicapillus*. We also estimate the amount of inertial reorientation due to wing arc and moment of inertia

asymmetries at different points in the wingbeat cycle. Based on our initial investigation (Hedrick and Biewener, 2007b), we hypothesized that the estimated change in orientation due to inertial effects would predominate during the wingbeat and that aerodynamic forces would have a greater influence on among-wingbeat changes in orientation.

Prior to the analysis presented in Hedrick and Biewener (Hedrick and Biewener, 2007b) and based on an earlier study of turning flight in pigeons (Warrick and Dial, 1998), we hypothesized that the pectoralis would be the key muscle for control of maneuvering flight. However, we then discovered that much of the link between wrist velocity and change in roll rested on inertial relationships that might have only a small effect over a complete wingbeat cycle. This suggested that other muscles might also play an important role in turning flight, as was reported in an earlier electromyographic and kinematic study of pigeons maneuvering through a slalom course (Dial and Gatesy, 1993). We therefore hypothesized that all four muscles examined, the pectoralis, supracoracoideus, biceps brachii and extensor metacarpi radialis, contribute to different factors related to aerodynamic and inertial reorientation. The biceps brachii influences wing rotation on the spanwise axis and therefore angle of attack (Dial and Gatesy, 1993), contributing to aerodynamic asymmetry. The pectoralis, the main source for muscular force and power during the downstroke in flapping flight, was previously shown to be important in inertial reorientation (Hedrick and Biewener, 2007b). The supracoracoideus, the main wing elevator and a key supinator during upstroke (Poore et al., 1997b), likely influences the arc swept by the wing and therefore both inertial and aerodynamic forces. Finally, the wrist extensor influences both wing area and distal wing moments of inertia, which are also likely to influence aerodynamic torque and inertial reorientation forces, respectively.

Materials and methods

Aside from the differences noted in this section, the kinematic and electromyographic data used in this analysis were identical to those described in the companion paper (Hedrick and Biewener, 2007b). The methods of data reduction, kinematic frames of reference, and EMG processing were also identical except where otherwise noted.

Wing and body kinematics

In addition to the points digitized previously on the cockatoos *Eolophus roseicapillus* Viellot (Hedrick and Biewener, 2007b), we also digitized the trailing edge of the wing at the tips of the 4th primary and 1st secondary feathers. These points were digitized only at mid-downstroke when the wing was fully extended and the individual feathers were easily identified by counting in from the tip; the trailing edge points could not be accurately identified at other points in the wingbeat cycle. However, flight muscle and therefore aerodynamic forces are greatest at mid-downstroke (Hedrick et al., 2003), making mid-downstroke the most characteristic point in a wingbeat cycle.

Aside from the EMG plug base and the trailing edge points described above, the cockatoos were digitized only at the end of downstroke, mid-upstroke, the start of downstroke, and the seven frames surrounding mid-downstroke. These four points in the wingbeat cycle were identified visually from the video sequences; we include a series of still images showing typical body and wing posture at each stage (Fig. 1).

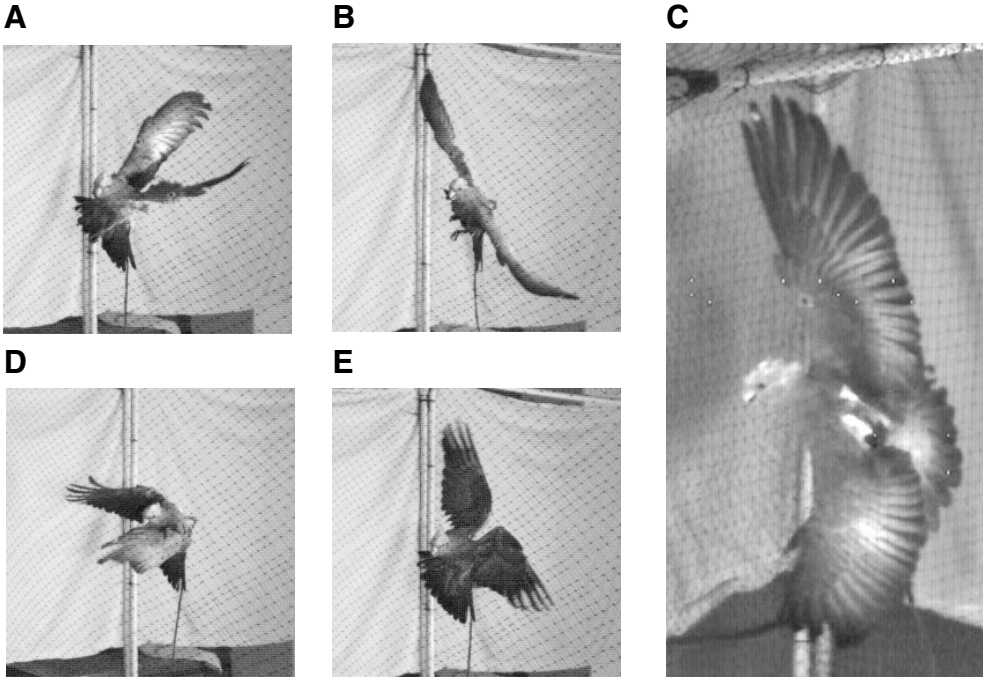

Fig. 1. Characteristic wing orientation at (A) the start of downstroke, (B,C) mid-downstroke, (D) the end of downstroke and (E) mid-upstroke. We judged downstroke to begin when the tips of the primaries were rapidly accelerated by downward angular acceleration beginning at the shoulder, as is visible in the tips of the right wing primaries in A. Mid-downstroke was the moment of greatest angular extent between the two wings. The end of downstroke was judged to occur as just prior to the wrists beginning an upward trajectory. Finally, we considered mid-upstroke to be the frame in which the angle defined by the wrists first reach their maximum upward excursion.

A blade-element model of aerodynamic force and torque

We used a blade-element model to estimate the aerodynamic forces and torques generated by the cockatoos' wings at mid-downstroke. This mid-downstroke estimate was then used as a basis for estimating the force and torque impulses delivered during the entire wingbeat. While blade-element models have a long history in biological flight research (e.g. Osborne, 1951; Ellington, 1984), recent advances in measurement of the aerodynamic coefficients appropriate for rotating wings enhance their applicability to kinematic studies of animal flight (Sane, 2003). While the majority of these examples are from insect flight and at lower Reynolds numbers (~100 to ~2000) than those characteristic of the cockatoos (~26 000), Usherwood and Ellington (Usherwood and Ellington, 2002b) found high force coefficients for revolving quail wings, also at a Reynolds number of ~26 000.

In the blade-element approach used here, we first divided the wings of four cockatoos into 1 cm wide strips, measuring the area of each strip and combining the results from the four birds into a single standard wing [table 3 in the companion paper (Hedrick and Biewener, 2007b)]. The velocity of the *i*th segment (V_i) at mid-downstroke was calculated as:

$$\vec{V}_i = d_i \frac{\vec{V}_{b,wrist}}{d_{wrist}} + \vec{V}_{bird}\,, \qquad (1)$$

where d_i is the distance from the shoulder to the midpoint of the *i*th segment of the standard wing, $\vec{V}_{b,wrist}$ is the velocity of the wrist in the body coordinate system, d_{wrist} the distance from the shoulder to the wrist segment in the standard wing, and $\vec{V}_{bird}$ the velocity of the EMG plug attachment site in the global coordinate system (Fig. 2). Note that the blade-element velocity calculation, Eqn 1, assumes still air and does not incorporate any estimate of the effect of induced velocity on overall flow direction or magnitude. However, we compensated for this by using aerodynamic force coefficients derived from data that relate angles of attack, also computed assuming still air, to forces measured with fully developed induced velocity (see below).

The position of each wing segment in the body coordinate system, $\vec{r}_{b,i}$, was estimated as:

$$\vec{r}_{b,i} = d_i \frac{\vec{r}_{b,wrist}}{d_{wrist}}\,, \qquad (2)$$

where $\vec{r}_{b,wrist}$ is the position vector of the wrist in the body coordinate system.

The direction of aerodynamic force acting on each wing segment was determined by assuming that the net aerodynamic force on a wing was directed orthogonal to the upper surface of the wing (Usherwood and Ellington, 2002a). A coefficient of net force was estimated for each segment from empirical measurement of the force coefficients on a revolving quail wing (Usherwood and Ellington, 2002b) and an estimate of the angle of attack of each segment (Eqn 3). Although the wings of the cockatoos studied here have a greater aspect ratio than the quail wings studied by Usherwood and Ellington (Usherwood and Ellington, 2002b), variation in wing shape parameters had little influence on the force coefficients measured from revolving wings (Usherwood and Ellington, 2002b).

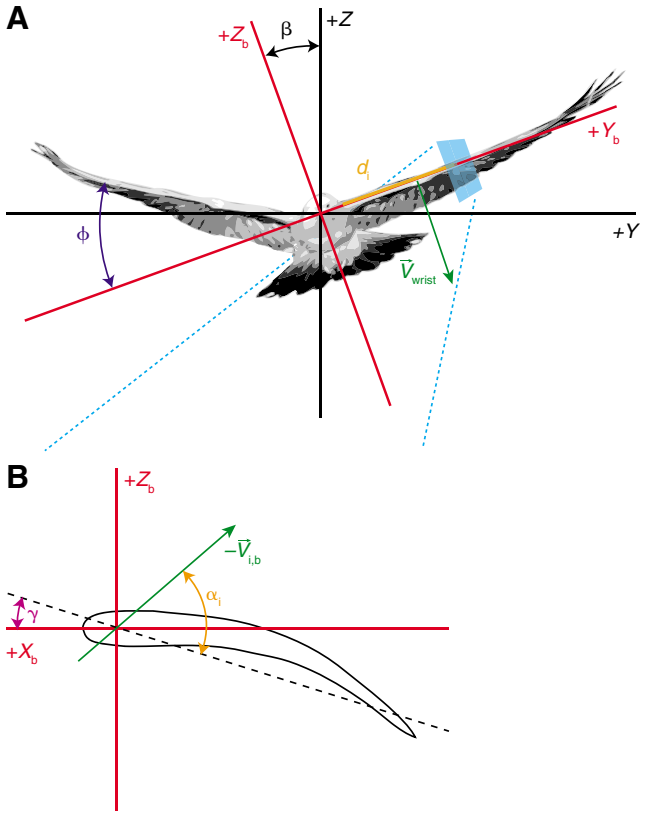

Fig. 2. Frames of reference and characteristic angles used in the blade-element analysis. (A) The bird at mid-downstroke, along with the bird's right wing from an earlier instant in the stroke, the global and bird coordinate systems, and several orientation parameters. Note that the wing elevation angle, ϕ, is shown for the wing position at the prior instant in time as ϕ at mid-downstroke is approximately 0°. (B) A wing section and associated angles. Note that γ, the wing spanwise rotation angle, is slightly negative as shown. Additionally, $\vec{V}_i$ has been transformed to the body coordinate system to give $\vec{V}_{i,b}$ (see List of symbols and abbreviations).

The wing surface orientation, for use with the normal forces assumption and determination of angle of incidence, was computed from the X_b and Z_b components of the normal vector to the plane defined by the positions of the wrist, tip of the 4th primary and tip of the 1st secondary, giving a spanwise rotation angle, γ, for the entire wing (Fig. 2B).

This spanwise rotation angle was combined with an estimate of the flow velocity for each segment, $\vec{V}_i$, computed by applying the roll, pitch and yaw rotations to the $\vec{V}_i$, the result of Eqn 1. The chordwise components of the estimated flow were combined with spanwise wing rotation angle to compute the wing's angle of attack, α_i (Fig. 2B):

$$\alpha_i = \cos^{-1}\left(\frac{-\vec{V}_{b,i}\bullet[\cos\gamma,0,\sin\gamma]}{|\vec{V}_{b,i}|}\right), \qquad (3)$$

where the zero in the [cosγ,0,sinγ] orientation vector enforces

computation of the angle of attack from chordwise flow only, assuming that chordwise flow is in the X_bZ_b plane. This assumption is reasonable at mid-downstroke, when the wings are extended along the Y_b axis, but not at other points within the wingbeat cycle. The angles of attack (α_i) were converted to coefficients of resultant force ($C_{r,i}$) using the following equation, generated by a polynomial fit to the data in (Usherwood and Ellington, 2002b) for real and model quail wings in steady state rotation:

$$C_r = -2.414\alpha^3 + 4.835\alpha^2 - 0.051\alpha + 0.118 , \quad (4)$$

where α is the angle of attack in rad. The range of α in the data used to create the fit extend from –0.4 to 1.25 rad. These high force coefficients derived from measurement of revolving wings allow estimation of the forces due to three-dimensional and unsteady aerodynamic effects and are thus appropriate for slow, flapping flight (Sane, 2003).

The results of these equations were combined to provide a net estimated force vector for the wing as a whole:

$$\vec{F}_{est} = \frac{1}{2}\rho\sum_{1}^{n} C_{r,i}s_i|\vec{V}_i|^2[\cos\gamma,0,\sin\gamma] , \quad (5)$$

where ρ is air density and s is wing area, as well as an estimated torque vector $\vec{\tau}_{est}$ for the wing:

$$\vec{\tau}_{est} = \frac{1}{2}\rho\sum_{1}^{n} \vec{r}_{b,i}\times C_{r,i}s_i|\vec{V}_i|^2[\cos\gamma,0,\sin\gamma] , \quad (6)$$

where $\vec{r}_b$ is position vector in the body coordinate system.

To extend $\vec{F}_{est}$ from mid-downstroke to a mean force for the entire stroke, we made the following assumptions: (1) aerodynamic force is generated only during the downstroke and (2) aerodynamic force in downstroke varies as a half-sine, peaking at mid-downstroke. These assumptions are consistent with measurements of pectoralis force production (Dial and Biewener, 1993; Biewener et al., 1998; Hedrick et al., 2003) and the time course of wing pressure distribution (Usherwood et al., 2005). Under these assumptions, the average force produced by the bird during the entire stroke is:

$$\bar{\vec{F}} = \frac{2}{\pi}\frac{t_{ds}}{t_{ws}}\vec{F}_{est} , \quad (7)$$

where t_{ds} is the downstroke duration, and t_{ws} is the whole stroke duration. We extended the estimated torque, $\vec{\tau}_{est}$, to estimated mean torque, $\bar{\vec{\tau}}_{est}$, using an identical approach.

Estimating upward aerodynamic force

To verify the accuracy of forces and torques estimated by the above equations, we also used the blade-element model to estimate the upward component of aerodynamic force for comparison with the bird's weight. For non-accelerating flight, the upward aerodynamic force produced over an integer number of wingbeats should equal the bird's weight. As before, we assumed that aerodynamic force varied as a half sine wave during downstroke, peaking at mid-downstroke, the point at which we estimated force from the kinematic data using Eqn 5. We also assumed that forces on the wing were oriented normal to the upward surface, and corrected for force orientation due to the measured spanwise rotation, γ, and changes in wing elevation (or dihedral) angle, ϕ, through the stroke. Elevation angle was assumed to vary from 45° above horizontal in the body coordinate system to 45° below. Finally, we assumed that forces were generated only during downstroke (Hedrick et al., 2004). These assumptions were expressed as:

$$\bar{F}_z = F_{z,est}\cos\beta\left(\frac{t_{ds}}{t_{ws}}\right)\left(\frac{4\sqrt{2}}{3\pi}\right) , \quad (8)$$

where $F_{z,est}$ is the upward component of $\vec{F}_{est}$, β is the roll angle at mid-downstroke (Fig. 2), and $4\sqrt{2}/3\pi$ is the average of the curve $y=\sin(x)\sin[(x/2)+(\pi/4)]$ for x from 0 to π, the combination of the assumed sinusoidal variation of force and elevation angle through the downstroke. Note that Eqn 8 is for one wing only; we therefore summed the mean forces from the left and right wings to obtain the total net upward aerodynamic force.

Estimating inward aerodynamic force and mechanical power

The mean inward, i.e. centripetal aerodynamic force was estimated with a similar process, substituting only sine β for cosine β in Eqn 8. Rather than overcoming gravity, the inward force generated by the wings must provide the centripetal force required to change heading. The mean centripetal force for a wingbeat was estimated from the data as follows:

$$\bar{F}_c = M\frac{\bar{u}^2}{r} , \quad (9)$$

where M is body mass, r is turn radius, and $\bar{u}$ is the bird's average flight speed during the turn. Turn radius was computed as:

$$r = \frac{\bar{u}t_{ws}}{\Delta\psi} , \quad (10)$$

where $\Delta\psi$ is the change in heading or flight path during the stroke.

The mechanical power P required to generate the aerodynamic forces was estimated as:

$$P = \frac{1}{t_{ws}}\lambda\frac{1}{\pi}\rho\sum_{1}^{n}|\vec{r}_{b,i}|C_{r,i}s_i|\vec{V}_i|^2d_i , \quad (11)$$

where λ is the arc swept by the wing during downstroke. The estimated power was calculated by combining our estimate of aerodynamic force (Eqn 5) with the distance moved by each wing segment during downstroke and the duration of the entire wingbeat. The estimate formulated in Eqn 11 assumes that the wing flaps with a constant angular velocity during downstroke, an assumption supported by *in vivo* measurements of muscle length change in the avian pectoralis during flight (e.g. Askew et al., 2001; Hedrick et al., 2003). These studies note both an initial rapid shortening and later slow shortening phase of muscle contraction during downstroke, but the overall muscle lengthening – shortening cycle was best described as a

sawtooth, rather than sinusoidal wave (Askew and Marsh, 2001). Alternatively, assuming that wing angular velocity varies sinusoidally during the stroke would increase the estimated mechanical power by a factor of $\pi^2/8$, or approximately 23%.

Inertial reorientation

As was shown in the companion paper (Hedrick and Biewener, 2007b), both instantaneous and net inertial changes to orientation are likely in avian maneuvering flight. The degree of both these effects is related to the moments of inertia of the wing through time and the arc swept by the wing over the course of the wingbeat cycle. Here we show how measurements of wing position at four different points within the wingbeat cycle were used to estimate the magnitude of these inertial effects. First, for each wing at each of the four positions (see Fig. 1) we computed the wing moment of inertia with respect to the X_b or roll axis for rotation about its shoulder joint:

$$I_{\text{wing,s}} = \sum_{1}^{n} M_i d_{\text{yz,i}}^2 , \quad (12)$$

where M_i is the mass of the ith wing section and $d_{y,i}$ is its distance from the shoulder joint in the Y_bZ_b plane. Distances from the shoulder were computed for each section by evenly distributing the proximal wing sections along the shoulder–wrist segment and the distal wing sections along the wrist–tip segment. We also used a similar formula to compute an $I_{\text{wing,o}}$, the moment of inertia for rotation about the opposite shoulder joint. We then estimated the wing moment of inertia during a stroke interval as the average of the wing moment at the interval end points. As shown in Appendix 1 of the companion paper (Hedrick and Biewener, 2007b), these were combined with the change in elevation angle through which each wing moved during the specified stroke interval to give an estimate of inertial body roll during that interval:

$$\Delta\beta = \frac{\bar{I}_{\text{rwing,s}}\Delta\phi_{\text{rwing}}}{(I_{\text{body}} + I_{\text{lwing,o}})} - \frac{\bar{I}_{\text{lwing,s}}\Delta\phi_{\text{lwing}}}{(I_{\text{body}} + I_{\text{rwing,o}})}, \quad (13)$$

where $\Delta\phi_{\text{wing}}$ is the elevation angle change for the wing during the interval of interest and an r or l prefix in the subscript indicates the right or left wing. The predicted change in body roll over a complete wingbeat was estimated as the sum of $\Delta\beta$ for the start of downstroke to mid-downstroke, mid-downstroke to end of downstroke, end of downstroke to mid-upstroke, and mid-upstroke to end of upstroke sequence.

Statistics

General results characteristic of the entire turning flight were computed as the inter-individual mean of the six cockatoos. Regression and partial correlation tests against kinematic data were computed from the standardized wingbeats from each of the cockatoos in each of the turn directions, resulting in N of ~66 (six cockatoos, six wingbeats when turning left, five wingbeats when turning right). Regression and partial correlation tests against EMG data were computed from the standardized EMG differences, resulting in N of ~30 in each comparison. All computations were performed in MATLAB 7.0 (Mathworks Inc., Natick, Massachusetts).

Results

Aerodynamic force, torque and power estimates

We found that the estimated net aerodynamic torque at mid-downstroke was a significant predictor of roll acceleration (r^2=0.55, P<0.00001, Fig. 3). This made it a more informative predictor than right–left asymmetry in wrist velocity, the basic kinematic parameter most closely related to roll acceleration, which predicted roll acceleration with an r^2 of 0.34 (Hedrick and Biewener, 2007b).

The estimated mean upward force was 2.47±0.58 N (N=6). This corresponds to 88±17% (N=6) of the force required to support the bird in the air. Vertical force also varied through the turn, reaching a local minimum at the 0th wingbeat, the middle wingbeat of the turn (Fig. 4).

Centripetal acceleration varied widely among the wingbeats that made up the turn, but was on average 8.37±1.95 m s^{-2} (N=6). Centripetal acceleration was greatest during the 0th wingbeat of the turn, with an inter-individual mean of 10.86±2.79 m s^{-2} (N=6). Not surprisingly, the inward aerodynamic force providing centripetal acceleration also varied widely among wingbeats, and reached a maximum at the 0th wingbeat (Fig. 5). The estimated mean inward force generated during each wingbeat was somewhat less than the product of centripetal acceleration and body mass for each cockatoo (Fig. 5). On average, the estimated inward force accounted for 79±29% (N=6) of the centripetal force required to produce the observed change in heading.

Aerodynamic power varied slightly among wingbeats in the turn and among individual birds. The overall mean estimated aerodynamic power was 13.48±4.23 W (N=6), which

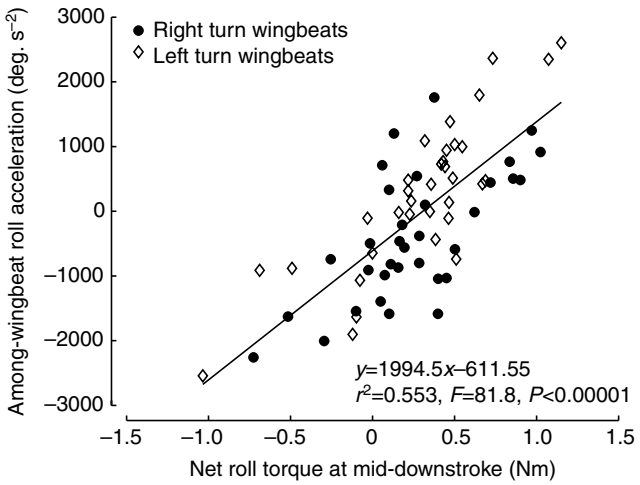

Fig. 3. Individual points are the average response of a bird for a given wingbeat number and turn direction, N=68. Net roll torque was estimated *via* a blade-element analysis, among-wingbeat roll acceleration from the second derivative of a quintic spline fit through the series of mid-downstroke roll measurements.

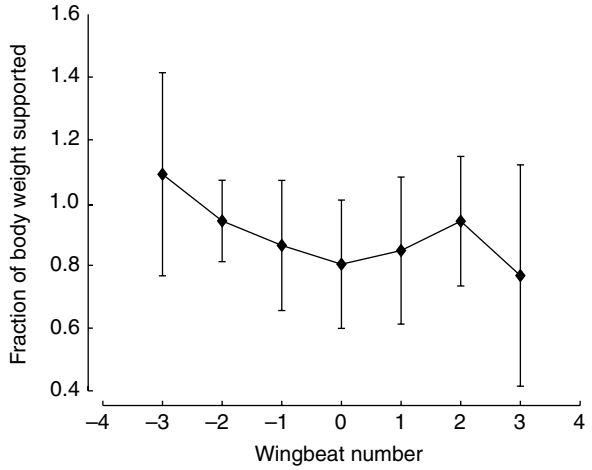

Fig. 4. Inter-individual mean fraction of body weight supported during each wingbeat of the turn (N=6 for each wingbeat). Fraction of body weight supported was calculated by dividing the estimated mean upward force generated each bird by its body weight. The overall average fraction supported was 0.89. The fraction supported reaches a local minimum at the 0th wingbeat, the middle wingbeat of the turn and also the one with the greatest average body roll.

corresponds to a pectoralis mass-specific power of 233.2±65.8 W kg^{-1} (N=6). Power was greatest at the middle wingbeat of the turn and tended to decline by the last wingbeat as the birds approached the landing perch (Fig. 6).

Inertial reorientation estimates

The predicted inertial reorientations for each phase of the wingbeat cycle were significantly related to measured reorientation during that phase (Fig. 7). However, the degree of correlation between the inertial predictions and actual reorientation was moderate and varied among phases, ranging from r^2=0.37 for the mid-upstroke to start of downstroke phase to r^2=0.20 for the end of downstroke to mid-upstroke phase. The slopes and intercepts of the linear regression lines averaged 1.19° and –1.07°, respectively. Thus, our predictions of change in orientation over these subsections of the wingbeat cycle were of similar magnitude to the measured changes. When summed over an entire wingbeat, the predicted inertial changes in body roll were significantly but moderately (r^2=0.19) related with the measured change in roll (Fig. 8). As before, the regression slope and intercept were near one and zero, respectively.

Muscle activation parameters: aerodynamic reorientation

Although we found no individual muscle activation parameters that explained or were correlated with either the net aerodynamic torque or inertial reorientation summed over an entire wingbeat, we found many relationships between muscle activation measurements and different components of our aerodynamic and inertial reorientation estimates. These relationships are summarized in Table 1 and noted below. The outside wing–inside wing difference in spanwise rotation angle (γ) was significantly related to the outside–inside difference in pectoralis EMG intensity (r^2=0.331, P<0.005, F=12.9) such that greater EMG intensity was associated with upward rotation of the trailing edge. The outside–inside difference in the supracoracoideus rectified impulse was also correlated with spanwise rotation (r^2=0.247, P=0.01, F=8.2) such that greater supracoracoideus EMG was associated with downward rotation of the trailing edge, an increase in the spanwise rotation angle. Biceps activation duration was correlated with spanwise rotation angle at mid-downstroke (r^2=0.273, P=0.015, F=9.4, Fig. 9), with greater activation duration associated with greater spanwise rotation (trailing edge down, supination). The square of wing velocity in the world coordinate system was correlated with

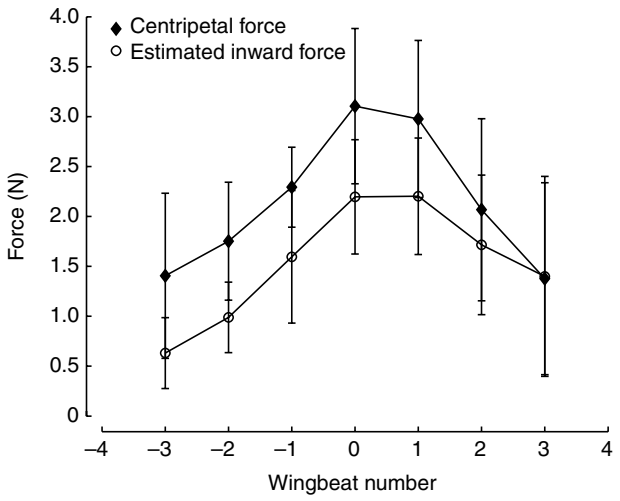

Fig. 5. Inter-individual centripetal force and estimated mean inward aerodynamic force for each wingbeat during the turn. Across all wingbeats and birds the estimated inward force accounted for 72±18% of the observed centripetal force (N=67).

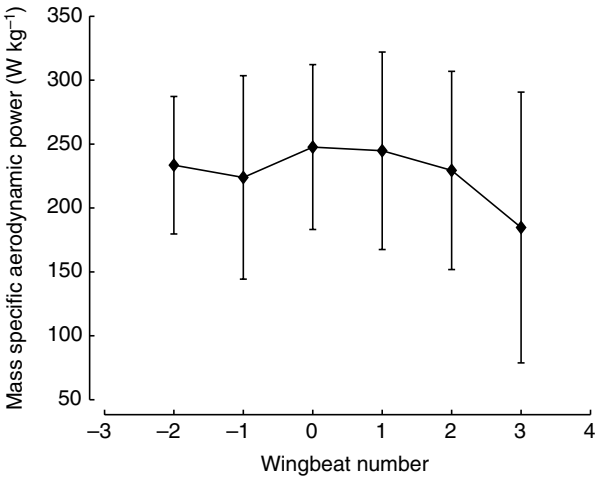

Fig. 6. Pectoralis mass specific aerodynamic power estimated from the wing kinematics at mid-downstroke, stroke duration and wrist arc during downstroke, shown as the inter-individual mean ± s.d. Across all birds and wingbeats, power averaged 238.24±80.85 W kg^{-1} (N=58). Note that data for wingbeat –3 were not available because a stroke duration, measured from mid-upstroke to mid-upstroke, was not available from 4 of the 6 birds.

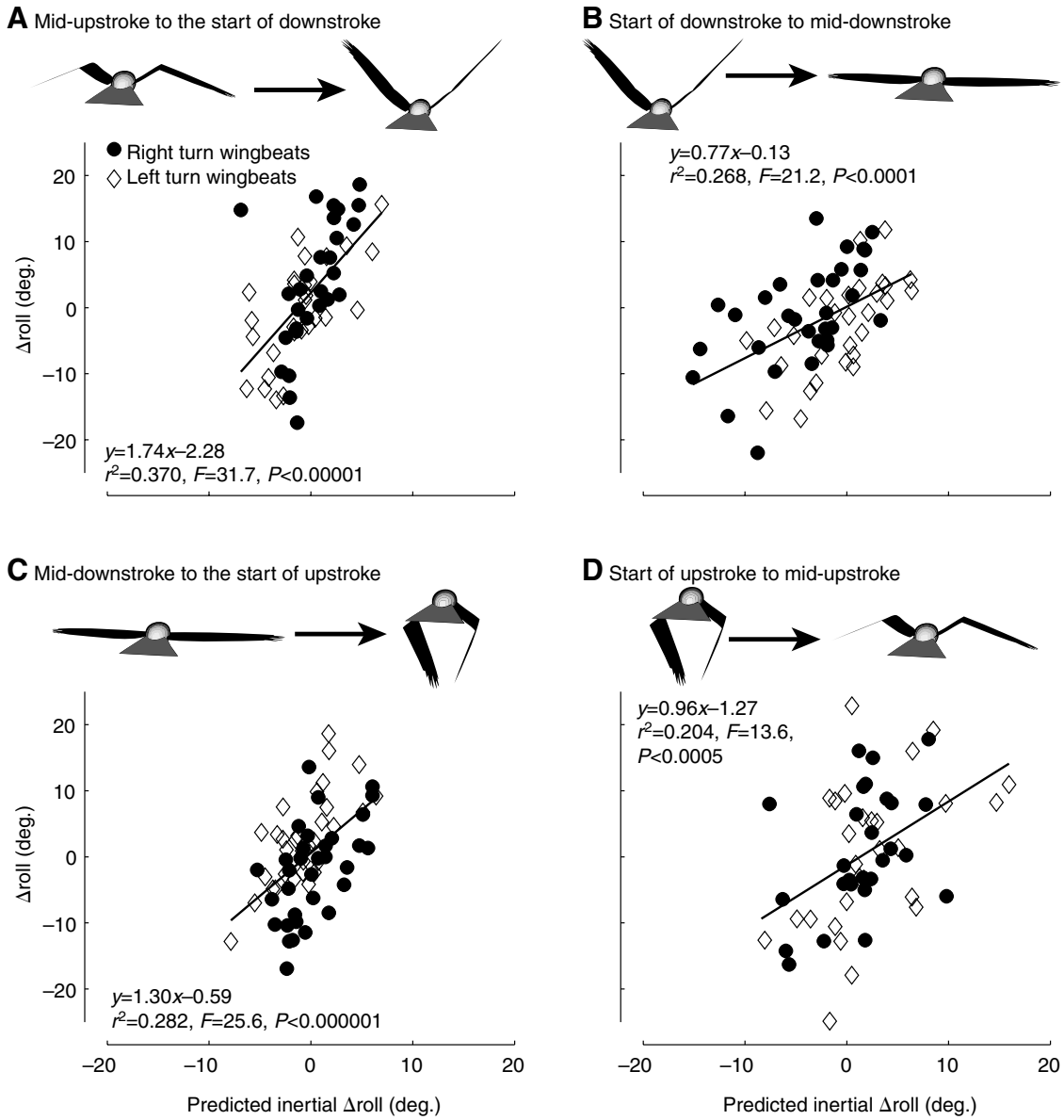

Fig. 7. Predicted *versus* measured change in roll during the four phases of the wingbeat cycle. (A) Mid-upstroke to the start of downstroke, (B) the start of downstroke to mid-downstroke, (C) mid-downstroke to the end of downstroke, (D) the end of downstroke to mid-upstroke. Because the inertial predictions do not take into account any initial roll velocity, we high-pass filtered the measured roll angles with a cut-off frequency of 3.5 Hz prior to computing the change in roll for comparison with the inertial predictions.

pectoralis time to mid-burst, an expression of muscle activation delay (r^2=0.433, P<0.0001, F=22.1) such that increased time to mid-burst was associated with increased wing velocity at mid-downstroke. Finally, we found that increased pectoralis activation intensity was correlated with greater aerodynamic force coefficients (r^2=0.277, P<0.005, F=9.6, Fig. 9).

Muscle activation in relation to inertial reorientation

We did not find a significant correlation between any individual muscle activation parameter and inertial reorientation over a complete stroke. However, inertial reorientation during discrete portions of the wingbeat was often related to one or several muscle activation parameters. Inertial reorientation from mid-upstroke to the start of downstroke was significantly correlated to the duration of supracoracoideus activation (r^2=0.446, P<0.0005, F=20.2, Fig. 9), with longer activation durations corresponding to inertial reorientation toward the same side.

Three different muscles were significantly related to inertial reorientation of roll from the start to the middle of downstroke. A larger biceps EMG impulse was associated with inertial roll to the same side (r^2=0.379, P<0.001, F=15.3, Fig. 9). The mean spike amplitude of the wrist extensor was inversely correlated with inertial reorientation (r^2=0.420, P<0.0005, F=18.1). Finally, the pectoralis mean spike amplitude was also inversely correlated with inertial reorientation in early downstroke

(r^2=0.322, P<0.005, F=11.4). Inertial reorientation from the middle to the end of downstroke was positively correlated with only one EMG parameter, the duration of pectoralis activation (r^2=0.292, P<0.005, F=10.3).

Discussion

We found that both aerodynamic and inertial mechanisms contribute to the changes in roll orientation that underlie low speed turning in the rose-breasted cockatoo. Predicted within-wingbeat inertial roll reorientations were significantly related to measured reorientations (Fig. 7). Estimated aerodynamic torque at mid-downstroke was a good predictor of among-wingbeat roll acceleration (Fig. 3). Furthermore, the estimated mean upward and inward aerodynamic forces were good matches to body weight (Fig. 4) and centripetal force (Fig. 5), respectively. Finally, several of the factors that contributed to the estimates of both aerodynamic torque and inertial reorientation were correlated with specific muscle activation measurements, providing some insight into how the neuromuscular system manages changes in heading and orientation in avian flight. These EMG results support an integrated model of neuromuscular control of maneuvering, where all aspects of the flight apparatus are modulated.

Inertial roll reorientation within a wingbeat

As noted above, inertial reorientation was a major factor in determining within-wingbeat changes in roll. In each of the four phases of the wingbeat cycle, our estimates of inertial reorientation were significantly related to the measured change in roll (Fig. 7). The correlation was not particularly strong in some cases, especially from the end of downstroke to mid-upstroke; this may be due to the poor temporal resolution of our wing moment of inertia estimates. Because we measured moment of inertia at only four instants throughout the wingbeat cycle, we used an average of the two instants defining an interval to characterize wing moment of inertia for the entire interval. This simplification, along with changes in orientation due to non-inertial factors (i.e. aerodynamic forces), likely accounts for much of the error in our inertial predictions.

Within-wingbeat inertial changes in orientation may play an important role in maneuvering flight, especially in generating changes in heading smaller than those studied here. Because the aerodynamic force experienced by the wings varies widely over the course of a wingbeat, inertial reorientation that leads to a change in roll at mid-downstroke would cause a lateral aerodynamic force, a lateral acceleration and a change in heading. This change would come with the added advantage that the net change in roll would be slight to non-existent, leaving the bird well oriented for steady flight or another slight change in direction during the next wingbeat.

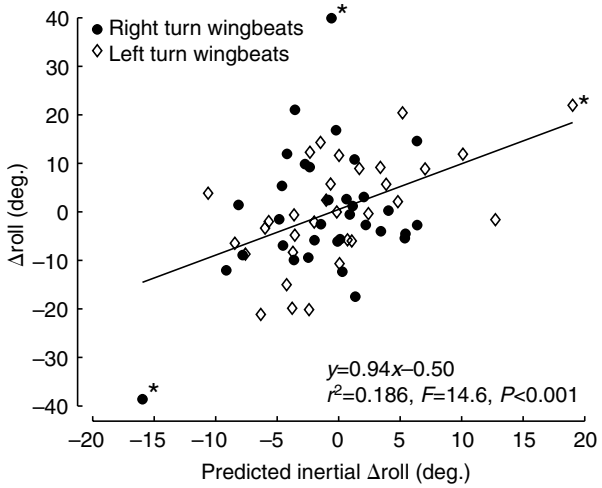

Fig. 8. Predicted *versus* estimated inertial change in roll for an entire wingbeat. As in Fig. 6, roll measurement was subjected to a high-pass filter prior to extracting the measurement. Note that this particular regression includes three points (marked by asterisks) that are more than three standard deviations from the mean of at least one of the axes. Removing these points would reduce the r^2 of the regression to 0.089 and the P value to P=0.02.

Inertial roll reorientation among wingbeats

Although inertial roll reorientation within a wingbeat may be sufficient for some maneuvers, the cockatoos studied here rolled into the turn over the course of several wingbeats [see fig. 9 in the companion paper (Hedrick and Biewener, 2007b)]. Inertial reorientation can also contribute to these changes, although the rate of change in orientation will be less than that

Table 1. *EMG correlations to aerodynamic and inertial reorientation components*

	Pectoralis	Supracoracoideus	Biceps	Ext. metacarpi radialis
Aerodynamic				
Spanwise rotation angle	Negative	Positive	Positive	–
Aerodynamic force coefficient	Positive	–	–	–
Wrist velocity^2 (world CS)	Positive	–	–	–
Inertial				
Mid-upstroke to Start downstroke	–	Positive	–	–
Start to Mid-downstroke	Negative	–	Positive	Negative
Mid- to End downstroke	Positive	–	–	–

All relationships were significant with P ranging from <0.01 to <0.0001.

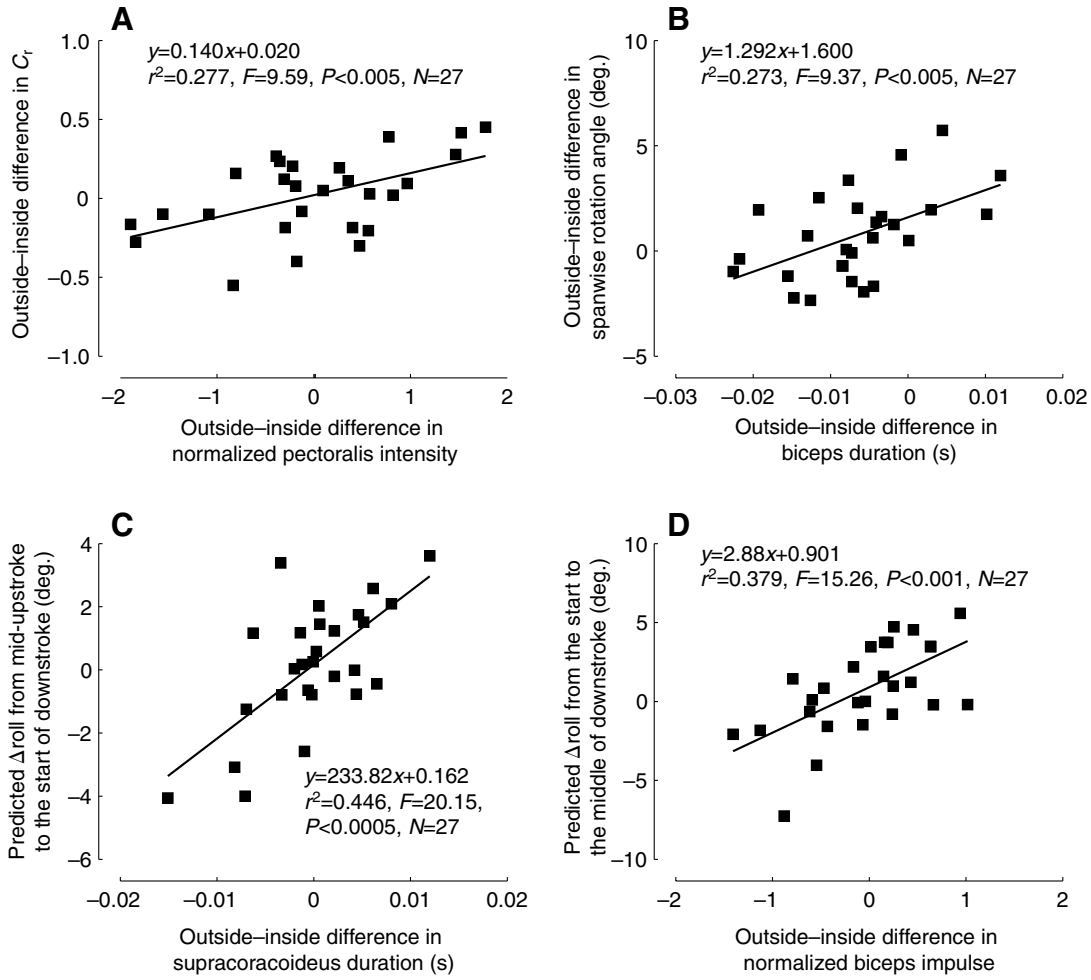

Fig. 9. Electromyogram correlates to different components of the estimated aerodynamic torque and the predicted change in roll due to inertial reorientation. Normalized EMG measures were normalized by dividing by the standard deviation of the measurement for the individual muscle. (A) Pectoralis activation intensity *versus* C_r, the aerodynamic force coefficient. (B) Biceps activation duration *versus* wing spanwise rotation at mid-downstroke. (C) Supracoracoideus activation duration *versus* the estimated inertial change in roll in late upstroke. (D) Biceps impulse *versus* the estimated inertial change in roll in early downstroke.

within a wingbeat. As for the within-wingbeat data, our estimate of inertial reorientation during a complete wingbeat was a significant although not especially strong correlate to the measured change in orientation (Fig. 8). As before, errors may be the result of the small number of moment of inertia measurements along with the accumulation of changes in orientation due to aerodynamic effects. Despite the weak correlation, the magnitude of the estimated net inertial changes to orientation (>10° per wingbeat) demonstrates that inertial reorientation cannot be ignored, even among wingbeats. The magnitude of estimated net inertial reorientation exceeds our initial estimates of ~2.0° (Hedrick and Biewener, 2007b) because the cockatoos simultaneously modulated both wing inertia and angular velocity, and because downstroke and upstroke arcs did not always match one another. For instance, a bird might sweep its wing through a 90° arc in downstroke but only a 60° arc in upstroke. This clearly has consequences for the subsequent downstroke, but leads to a larger net inertial roll reorientation in the interim.

Aerodynamic reorientation among wingbeats

Net aerodynamic torque, estimated from a blade-element analysis of the kinematic data, was a significant predictor of among-wingbeat roll acceleration (Fig. 3). Additionally, our extension of the model to estimate both mean upward and inward force for an entire wingbeat resulted in values close to the measured quantities. Specifically, the mean upward force from the blade-element analysis was 89% of body weight and the mean inward force was 72% of that required for centripetal acceleration during the turn. Finally, the mean aerodynamic power computed from the model, 238 W kg^{-1}, was within the range of pectoralis power measured from cockatiels flying in a wind tunnel (Tobalske et al., 2003) and blue-breasted quail in ascending flight (Askew et al., 2001). The match between the blade-element results and the measured flight forces, body weight and centripetal acceleration, demonstrates that the large aerodynamic coefficients, occasionally exceeding 2.0, drawn from measurement of the forces on a revolving quail wing

(Usherwood and Ellington, 2002b), likely reflect the actual force coefficients experienced by a bird wing in slow, flapping flight. Indeed, use of more moderate force coefficients such as those measured from bird wings held fixed in a wind tunnel (e.g. Withers, 1981) would leave the cockatoos severely deficient in mean upward and inward force, a result analogous to Ellington's proof by contradiction for the existence of unsteady aerodynamic effects in insect flight (Ellington, 1984). Here we find that low speed avian flight requires aerodynamic force coefficients greater than those obtained from bird wings positioned in a steady flow, suggesting that time-varying aerodynamic effects such as delayed stall are important in slow avian flight.

Aerodynamic torque, roll rate and damping

Despite our success in extending the blade-element estimates from mid-downstroke to whole stroke mean aerodynamic force and power, a similar approach did not give reasonable results for average torque, and thus angular acceleration, during the complete wing stroke. In fact, applying the approach outlined in Eqn 7 for estimating the mean roll acceleration from the instantaneous torque resulted in roll accelerations tenfold greater than those measured. However, our success of applying similar assumptions to our estimates of mean force and power suggests that the core estimates of aerodynamic force at mid-downstroke are not in error, but that the assumptions used to extend the estimate to a mean for the entire stroke were not appropriate.

Our main assumption was that the torque asymmetry measured at mid-downstroke was a good proxy for the degree of torque asymmetry throughout the downstroke. However, when closely examining one of the primary factors used in estimating roll torque, the square of wrist speed in the global coordinate system, we found that differences at mid-downstroke were not characteristic of differences during the entire downstroke (Fig. 10). Instead, the relationships at mid-downstroke were reversed later in the downstroke. This change may be the result of roll damping in avian flight. Roll damping occurs when roll to one direction creates a torque opposing the roll. Consider the case shown in Fig. 10B. From early to mid-downstroke, the cockatoo generates a greater roll torque on the right wing, leading to body roll to the left. As the bird rolls, the left wing moves downward while the right wing moves upward, increasing the velocity of the left wing relative to the right and leading to the conditions seen at the end of downstroke in Fig. 10B. The increased relative velocity of the left wing leads to a counter-roll torque to the right; the right and left wings do not act mechanically (or aerodynamically) independently.

A high degree of roll damping is typical of airplane flight, in which roll velocity rapidly declines to zero once the applied torque ceases (Nelson, 1997). Unlike the velocity-based mechanism proposed above, the mediating factor for fixed-wing aircraft is the angle of attack asymmetry created by rotational velocity. This effect may add to the velocity changes shown in Fig. 10B, but our data were insufficient to measure angle of attack throughout an entire wingbeat cycle. The different sources of roll damping in fixed-wing and flapping flight suggest that the degree of damping may also vary substantially.

The degree of roll damping characteristic of these low speed turns can be estimated from the torque-to-roll relationship shown in Fig. 11. The change in roll rate due to both applied torque and roll damping is given by:

$$\frac{\mathrm{d}\dot{\beta}}{\mathrm{d}t} = K\dot{\beta} + \frac{\tau}{I_x}, \qquad (14)$$

where $\dot{\beta}$ is roll rate, K is the roll damping coefficient, I_x is the roll moment of inertia, and τ is the roll moment due to wing asymmetry. We assume as before that τ during downstroke is in the form of a half-sinusoid with a peak at the estimated torque asymmetry, with τ equal to zero during upstroke. The $K\dot{\beta}$ portion of Eqn 14 provides the counter torque that establishes the wrist velocity pattern shown in Fig. 10B. The general relationship between estimated roll moment and roll acceleration, averaged over a whole wingbeat, was given in the regression equation from Fig. 3:

$$\ddot{\beta} = -1964\tau_{est} - 630.6\ . \qquad (15)$$

This equation includes a constant term, an unlikely circumstance

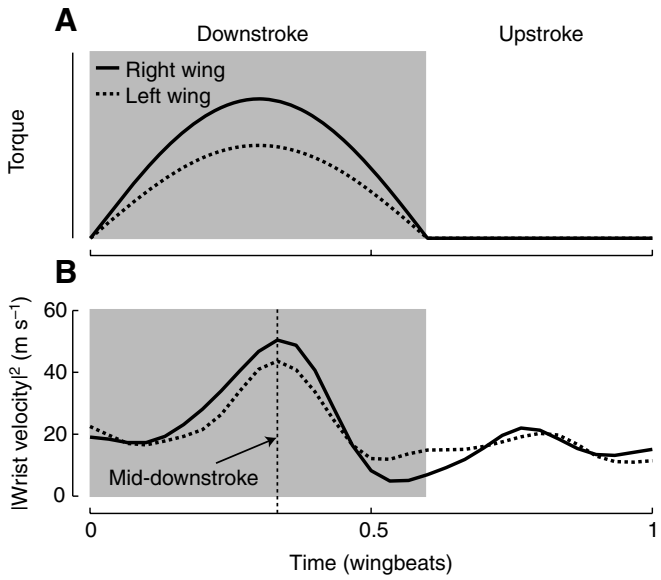

Fig. 10. (A) A depiction of how the assumptions used in extending the instantaneous measures of torque (or force) act over the course of a single wingbeat from the beginning of downstroke to the end of the subsequent upstroke. In the model, torque from the right wing is greater than that from the left wing during the entire downstroke. Note that torque due to upward force on the right wing has a negative sign; it was inverted to facilitate comparison with the left wing. (B) The square of the wrist velocity magnitude, an important part of our force and torque estimates. Note that the relationship between right and left torques at mid-downstroke does not persist through the entire stroke. The shading indicates downstroke in both modeled and recorded data; kinematic mid-downstroke does not occur at the temporal midpoint of the downstroke but downstroke did end at exactly 0.6 wingbeats in this instance.

since it implies that the cockatoos begin rolling with no wing asymmetry. This is unlikely, though not impossible if, for instance, the data cable applied torque to the bird. Given the unexpected appearance of the constant, we computed K for a τ=0.5 Nm and three separate equations relating $\ddot{\beta}$ and τ_{est}: (i) Eqn 15, (ii) Eqn 15 without the constant term, and (iii) a linear regression with no constant fit through the data in Fig. 3. In all cases we used the I_x for a bird with wings flexed [table 2 in the companion paper (Hedrick and Biewener, 2007b)]. These resulted in estimated K values (damping coefficients) of –60.32, –99.65 and –158.66 s^{-1}, respectively. For comparison between different individuals or species, K should be non-dimensionalized to C_K, a normalized damping coefficient, as follows:

$$C_K = K\frac{2I_x u}{Qsb^2}, \quad (16)$$

where Q is the dynamic pressure, u is flight speed, s is wing area and b is wing span (Nelson, 1997). Using the average values for these constants [tables 1 and 2 in the companion paper (Hedrick and Biewener, 2007b)] resulted in an estimated C_K of –1.14, –1.87 and –2.99 rad^{-1} for the respective cases. These values for C_K are 2–6 times greater than those typical of human piloted aircraft (Roskam, 1995). Thus, roll velocity will decay even more quickly in maneuvering birds than in airplanes. In fact, the time constants for these K are less than a wingbeat, so moderate roll velocities established at mid-downstroke will drop to near zero by the start of the next mid-downstroke. The greater roll damping experienced by flapping cockatoos as compared to fixed wing aircraft is likely due to the different sources of damping in the two types of flight. In fixed wing flight, roll damping is due to the largely linear relationship between angle of attack and aerodynamic force. In flapping flight, roll damping is due to the exponential relationship between the flow velocity over the wing and the resulting aerodynamic force.

This analysis of C_K, the normalized damping coefficient, cannot distinguish between an active counter-torque generated by asymmetric motion wing during upstroke or late downstroke and passive damping that would occur with symmetric wing kinematics. However, as noted above, rolling motion will enhance velocity on the outside wing during upstroke so a passive damping mechanism is plausible. The experimentally derived values for C_K are similar to those predicted by a simple model of roll damping in low speed flapping flight (Hedrick and Biewener, 2007a). Additionally, the flexible nature of the cockatoo's wings and body may enhance roll damping (Sneyd et al., 1982; Krus, 1997).

To assess the importance of aerodynamic torque to overall patterns of roll reorientation, we used the damped roll equation in combination with initial roll velocity, estimated mid-downstroke torque, and our assumption of sinusoidal torque during downstroke, to predict change in roll over an entire wingbeat. The resulting prediction was significantly correlated with the measured change in roll (r^2=0.213, P<0.0005, F=14.6, Fig. 11). The modest correlation is likely indicative of both errors in the initial estimate of net aerodynamic torque at mid-downstroke and variability in the damping coefficient K, both within and between wingbeats. Net inertial reorientation (Fig. 8) may also play a role, although estimated inertial reorientation was not a significant predictor of overall change in roll, either independent of estimated aerodynamic reorientation or when included as a co-predictor.

Electromyogram correlations to aerodynamic and inertial reorientation

The relationships between various EMG parameters and different factors important to aerodynamic and inertial reorientation, presented above and summarized in Table 1, generally agree with those uncovered in prior studies or evident from the simplified model of inertial reorientation presented in the companion paper (Hedrick and Biewener, 2007b). The association between pectoralis EMG intensity and spanwise rotation angle (γ) was such that greater EMG intensities correlated with upward rotation of the trailing edge of the wing, as might be expected given the position of the pectoralis insertion on the cranial margin of the humerus. Similarly, the relationship we found between increases in the supracoracoideus EMG rectified impulse and downward rotation of the trailing edge of the wing may be explained by the demonstration (Poore et al., 1997a) that the supracoracoideus imparts a substantial (supinating) rotation to the humerus. Persistence of this torque into early downstroke might influence wing orientation through the downstroke by changing the initial position of the wing before the pectoralis begins contracting. The correlation between increased biceps activation duration and increased downward (supinating) rotation of the trailing edge at mid-downstroke was consistent with that reported by Dial and Gatesy (Dial and Gatesy, 1993).

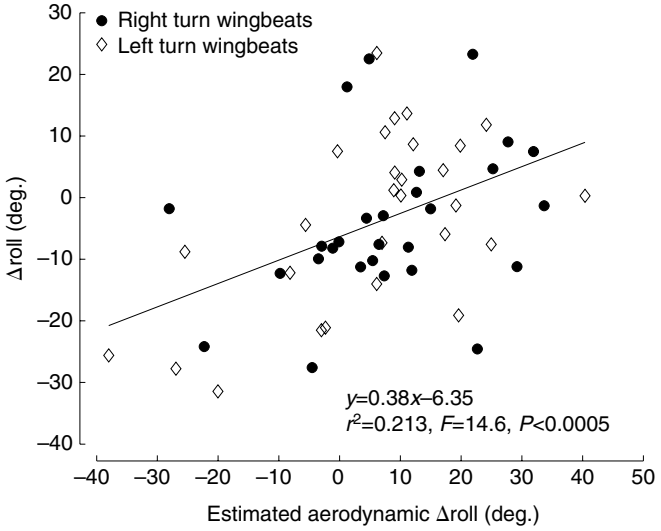

Fig. 11. Among-wingbeat change in roll *versus* the estimated aerodynamic effect, taking into account initial roll velocity and roll damping. The measured change in roll shown here is the total measured change, rather than the measured change in the higher frequency portion of the signal as was shown in Fig. 7 and compared with the predicted inertial reorientation.

Unlike the results described above, the positive correlation between pectoralis time to mid-burst and the square of wing velocity in the world coordinate system was somewhat counter-intuitive. We expected muscle activation parameters to relate most strongly to motion in the body frame of reference. However, the observed correlation may be explained by early activation of the pectoralis causing roll to the opposite side, which then appears as greater world coordinate system wing velocity on the side with the muscle activation delay. Finally, the association between greater pectoralis activation intensity and greater aerodynamic force coefficients was due to an association between greater pectoralis activation and greater downward-to-forward velocity ratio for the wing at mid-downstroke. This greater downward velocity influenced the angle of attack in opposition to the previously mentioned pectoralis influence on wing rotation, leading to a greater aerodynamic force coefficient.

Like the majority of the EMG to aerodynamic reorientation results described above, the relationships between the various EMG parameters and different aspects of inertial reorientation typically allowed simple interpretation. The positive correlation between inertial reorientation from mid-upstroke to the start of downstroke and the duration of supracoracoideus activation is consistent with the expected effect of a larger upstroke arc. For example, a longer activation of the right supracoracoideus might increase the elevation of the right wing relative to the left, leading to simultaneous inertial rotation toward the right. The correlation between increased biceps EMG impulse and inertial roll in the direction of the wing with elevated impulse is potentially the result of the biceps activity reducing the wing moment of inertia during downstroke. Likewise, the inverse correlation between wrist extensor mean spike amplitude and inertial roll could be the result of the wrist extensor increasing the wing moment of inertia. Finally, the inverse relationship between pectoralis mean spike amplitude and inertial roll in early downstroke is consistent with the expected inertial effects of a more rapid downstroke.

The positive relationship between pectoralis activation duration and inertial reorientation was initially more difficult to understand. We expected that greater activation duration would lead to a greater downward arc of the wing and therefore cause inertial reorientation toward the opposite side, leading to an inverse correlation. However, upon examination of the arcs, we found that greater pectoralis EMG duration was associated with net upward motion of the wrist during the final portion of downstroke. This may be due to the storage and release of energy in the supracoracoideus tendon at the end of upstroke (Hedrick et al., 2004), as greater energy storage could lead to a more rapid upstroke and therefore the observed net upward motion of the wrist. Alternatively, greater pectoralis activation was also associated inertial reorientation to the opposite side earlier in the downstroke (see above). Therefore, the observed reorientation toward the same side in the later half of downstroke may simply be a reaction to decelerating the faster moving wing. This relationship means that greater pectoralis activation in downstroke is initially correlated with inertial roll to the opposite side, then subsequently to the near side, for a small net effect over the entire downstroke.

Multiple EMG modalities enable turning flight

In the present study of rose-breasted cockatoos making 90° turns, we found that asymmetric pectoralis activation was involved in several aspects of both inertial and aerodynamic reorientation (Table 1 and above), although not to a degree sufficient to associate it with our overall predictions of net aerodynamic torque or inertial reorientation. As predicted in our initial examination of turning in cockatoos in the companion paper (Hedrick and Biewener, 2007b), all other flight muscles examined in this study were associated with at least one component of our estimates of inertial and aerodynamic reorientation. The extensive involvement of the main flight power muscles, the pectoralis and supracoracoideus, as well as the intrinsic wing muscles, demonstrates that flight control and maneuvering in birds is not managed by a discrete set of muscles but is, instead, an integrated system with effects distributed throughout the flight muscles. While it is likely that some of these muscles are more important to maneuvering than others, the experiments conducted here were insufficient to rank muscles in order of importance. Wing muscle denervation experiments performed on pigeons demonstrated that the birds were not capable of maneuvers such as landing and take-off without the use of their intrinsic wing muscles (Dial, 1992). Thus, we expect that the cockatoos would not be capable of turning without use of their intrinsic wing muscles. However, they may also not be capable of maneuvering without asymmetrically activating the pectoralis and supracoracoideus muscles. In summary, our results best support an integrated model of the neuromuscular control of maneuvering flight, where many components of the flight apparatus are modulated during maneuvering. This is in contrast to insect flight systems, where accessory muscles modulate the effects of flight motor muscles (e.g. Tu and Dickinson, 1994; Balint and Dickinson, 2004). The integrated control model also highlights differences between human engineered flight systems, with their limited set of actuators capable of generating variation in aerodynamic forces, and the vast range of aerodynamic and inertial reorientation possibilities open to animals with reconfigurable flapping wings.

Future work

This study points out a number of interesting avenues for further research. The possibility that birds may, in some circumstances, maneuver with primarily inertial rather than aerodynamic reorientations remains interesting and might occur in smaller amplitude, slalom-type turns where inertial reorientation over the course of a single wingbeat leads to sufficient change in heading. Additionally, assessing the importance of different morphological factors, such as wing area and wing moment of inertia, to maneuvering flight requires an integrated model that includes both aerodynamic and inertial reorientations along with velocity based damping. Finally, our understanding of the neural control of flapping

flight would benefit from studies recording muscle activation asymmetry over turns of different radii as well as perturbed turns where the bird's anticipated flight path was interrupted, forcing the bird to perform a rapid and unexpected maneuver.

List of abbreviations and symbols

b	wing span
C_r	resultant force coefficient
C_K	roll damping coefficient
d	distance
d_{wrist}	distance from the wing root to the wrist
$\vec{F}$	force vector
$\bar{\vec{F}}$	mean force vector for a complete wingbeat
F_z	upward force
F_c	centripetal force
I	moment of inertia
K	roll damping constant
M	mass
P	power
Q	dynamic pressure
r	turn radius
$\vec{r}_b$	position vector in the body coordinate system
s	wing area
t_{ds}	duration of downstroke
t_{ws}	duration of whole stroke
u	flight speed
$\vec{V}$	velocity vector in the global coordinate system
$\vec{V}_b$	velocity vector in the body coordinate system
α	angle of attack
β	roll angle
$\dot{\beta}$	roll velocity
$\ddot{\beta}$	roll acceleration
γ	wing spanwise axis rotation angle
λ	arc swept by the wing during a half-stroke
ρ	air density
τ	roll moment
$\vec{\tau}$	torque vector
$\bar{\vec{\tau}}$	mean torque vector for a complete wingbeat
ϕ	wing elevation angle
ψ	heading angle

We wish to thank the late Dr Russell Baudinette for facilitating this work at the University of Adelaide. Jayne Skinner and Craig McGowan also contributed enormously to the experiments; the work could not have been completed without their assistance. The manuscript was greatly improved by comments from Sanjay Sane and two anonymous referees. This project was funded by NSF IBN-0090265 to A.A.B.

References

Aldridge, H. D. J. N. (1987). Turning flight of bats. *J. Exp. Biol.* **128**, 419-425.

Askew, G. N. and Marsh, R. L. (2001). The mechanical power output of the pectoralis muscle of blue-breasted quail (*Coturnix chinensis*): the *in vivo* length cycle and its implications for muscle performance. *J. Exp. Biol.* **204**, 3587-3600.

Askew, G. N., Marsh, R. L. and Ellington, C. P. (2001). The mechanical power output of the flight muscles of blue-breasted quail (*Coturnix chinensis*) during take-off. *J. Exp. Biol.* **204**, 3601-3619.

Balint, C. N. and Dickinson, M. H. (2004). Neuromuscular control of aerodynamic forces and moments in the blowfly, *Calliphora vicina*. *J. Exp. Biol.* **207**, 3813-3838.

Biewener, A. A., Corning, W. R. and Tobalske, B. W. (1998). *In vivo* pectoralis muscle force–length behavior during level flight in pigeons (*Columba livia*). *J. Exp. Biol.* **201**, 3293-3307.

Dial, K. P. (1992). Avian forelimb muscles and nonsteady flight: can birds fly without using the muscles in their wings? *Auk* **109**, 874-885.

Dial, K. P. and Biewener, A. A. (1993). Pectoralis muscle force and power output during different modes of flight in pigeons (*Columba livia*). *J. Exp. Biol.* **176**, 31-54.

Dial, K. P. and Gatesy, S. M. (1993). Neuromuscular control and kinematics of the wings and tail during maneuvering flight. *Am. Zool.* **33**, 5.

Ellington, C. P. (1984). The aerodynamics of hovering insect flight. I. The quasi-steady analysis. *Philos. Trans. R. Soc. Lond. B Biol. Sci.* **305**, 1-15.

Frohlich, C. (1980). The physics of somersaulting and twisting. *Sci. Am.* **242**, 154-164.

Fry, S. N., Sayaman, R. and Dickinson, M. H. (2003). The aerodynamics of free-flight maneuvers in *Drosophila*. *Science* **300**, 495-498.

Hedrick, T. L. and Biewener, A. A. (2007a). Experimental study of low speed turning flight in cockatoos and cockatiels. *AIAA Paper* 2007-0044.

Hedrick, T. L. and Biewener, A. A. (2007b). Low speed maneuvering flight of the rose-breasted cockatoo (*Eolophus roseicapillus*). I. Kinematic and neuromuscular control of turning. *J. Exp. Biol.* **210**, 1897-1911.

Hedrick, T. L., Tobalske, B. W. and Biewener, A. A. (2003). How cockatiels (*Nymphicus hollandicus*) modulate pectoralis power output across flight speeds. *J. Exp. Biol.* **206**, 1363-1378.

Hedrick, T. L., Usherwood, J. R. and Biewener, A. A. (2004). Wing inertia and whole body acceleration: an analysis of instantaneous aerodynamic force production in cockatiels (*Nymphicus hollandicus*) flying across a range of speeds. *J. Exp. Biol.* **207**, 1689-1702.

Krus, P. (1997). Natural methods for flight stability in birds. *AIAA Paper* 97-5653.

Nelson, R. C. (1997). *Flight Stability and Automatic Control*. Boston, MA: McGraw-Hill.

Osborne, M. F. M. (1951). Aerodynamics of flapping flight with application to insects. *J. Exp. Biol.* **28**, 221-245.

Poore, S. A., Sanches-Haiman, A. and Goslow, G. E., Jr (1997a). Wing upstroke and the evolution of flapping flight. *Nature* **387**, 799-802.

Poore, S. O., Ashcroft, A., Sanchez-Haiman, A. and Goslow, G. E., Jr (1997b). The contractile properties of the m. supracoracoideus in the pigeon and starling: a case for long-axis rotation of the humerus. *J. Exp. Biol.* **200**, 2987-3002.

Roskam, J. (1995). *Airplane Flight Dynamics and Automatic Flight Controls*. Lawrence, KS: DARcorporation.

Sane, S. P. (2003). The aerodynamics of insect flight. *J. Exp. Biol.* **206**, 4191-4208.

Sneyd, A. D., Bundock, M. S. and Reid, D. (1982). Possible effects of wing flexibility on the aerodynamics of Pteranodon. *Am. Nat.* **120**, 455-477.

Tobalske, B. W., Hedrick, T. L., Dial, K. P. and Biewener, A. A. (2003). Comparative power curves in bird flight. *Nature* **421**, 363-366.

Tu, M. S. and Dickinson, M. H. (1994). Modulation of negative work output from a steering muscle of the blowfly *Calliphora vicina*. *J. Exp. Biol.* **192**, 207-224.

Usherwood, J. R. and Ellington, C. P. (2002a). The aerodynamics of revolving wings: I. Model hawkmoth wings. *J. Exp. Biol.* **205**, 1547-1564.

Usherwood, J. R. and Ellington, C. P. (2002b). The aerodynamics of revolving wings: II. Propeller force coefficients from mayfly to quail. *J. Exp. Biol.* **205**, 1565-1576.

Usherwood, J. R., Hedrick, T. L., McGowan, C. P. and Biewener, A. A. (2005). Dynamic pressure maps for wings and tails of pigeons in slow, flapping flight, and their energetic implications. *J. Exp. Biol.* **208**, 355-369.

Wagner, H. (1986). Flight performance and visual control of flight of the free-flying housefly (*Musca domestica* L.) I. Organization of the flight motor. *Philos. Trans. R. Soc. Lond. B Biol. Sci.* **312**, 527-551.

Warrick, D. R. and Dial, K. P. (1998). Kinematic, aerodynamic and anatomical mechanisms in the slow, maneuvering flight of pigeons. *J. Exp. Biol.* **201**, 655-672.

Warrick, D. R., Dial, K. P. and Biewener, A. A. (1998). Asymmetrical force production in the maneuvering flight of pigeons. *Auk* **115**, 916-928.